J Membrane Biol (2007) 216:117–127
DOI 10.1007/s00232-007-9047-7

Probing the Interaction Between KCNE2 and KCNQ1 in Their Transmembrane Regions

Xian-Sheng Liu · Mei Zhang · Min Jiang · Dong-Mei Wu · Gea-Ny Tseng

Received: 19 March 2007 / Accepted: 23 May 2007 / Published online: 4 August 2007

Abstract KCNE1-KCNE5 are single membrane-spanning proteins that associate with voltage-gated potassium channels to diversify their function. Other than the KCNQ1/KCNE1 complex, little is known about how KCNE proteins work. We focus on KCNE2, which associates with KCNQ1 to form K channels critical for gastric acid secretion in parietal cells. We use cysteine (Cys)-scanning mutagenesis to probe the functional role of residues along the KCNE2 transmembrane domain (TMD) in modulating KCNQ1 function. There is an α-helical periodicity in how Cys substitutions along the KCNE2 TMD perturb KCNQ1 pore conductance/ion selectivity. However, positions where Cys substitutions perturb KCNQ1 gating kinetics cluster to the extracellular end and cytoplasmic half of the KCNE2 TMD. This is the first systematic perturbation analysis of a KCNE TMD. We propose that the KCNE2 TMD adopts an α-helical secondary structure with one face making intimate contact with the KCNQ1 pore domain, while the contacts with the KCNQ1 voltage-sensing domain appear more dynamic.

Keywords Voltage-gated K channel – Mutagenesis · Structure-function relationship

Introduction

Members of the KCNE family (KCNE1-KCNE5) are single membrane-spanning proteins that can associate with voltage-gated cation (mainly potassium, or Kv) channels to modulate their single-channel conductance, gating kinetics and regulation by the cellular milieu (Abbott & Goldstein, 1998). The functional importance of KCNE1, KCNE2 and KCNE3 is supported by the linkage between inherited mutations in their genes and congenital diseases, such as cardiac arrhythmias, deafness and periodic paralysis (Abbott & Goldstein, 1998). Information about the structure-function relationship of KCNE subunits and the mechanism by which they modulate their partner Kv channel function is important for understanding their roles in physiology or pathology and for designing therapeutic agents targeting their actions.

KCNE1 associates with KCNQ1 to form the slow delayed rectifier (I_{Ks}) channels in the heart and inner ear (Sanguinetti et al., 1996). The KCNQ1/KCNE1 channel complex is the best-studied example of KCNE modulation of Kv channel function. KCNE1 increases KCNQ1 single-channel conductance, slows its activation, shifts the voltage dependence of activation in the positive direction and suppresses KCNQ1 inactivation (Sanguinetti et al., 1996; Sesti & Goldstein, 1998). To fulfill this function, KCNE1 seems to mainly rely on its transmembrane domain (TMD) and post-TMD region (Tapper & George, 2000; Wang, Tai & Goldstein, 1996; Wu et al., 2006b). Nuclear magnetic resonance (NMR) spectroscopy has suggested that the KCNE1 TMD adopts an α-helical structure (Aggeli et al., 1998). Furthermore, most KCNE1 positions where mutations can affect KCNE1 modulation of KCNQ1 function are found on one face of the putative transmembrane helix (Takumi et al., 1991; Goldstein & Miller, 1991; Wilson et al., 1994), suggesting that this may be the KCNE1 "interaction surface" when associated with KCNQ1 (Aggeli et al., 1998).

The other KCNE subunits share a high degree of amino acid sequence homology with KCNE1 in the TMD and

X.-S. Liu · M. Zhang · M. Jiang · D.-M. Wu · G.-N. Tseng (✉)
Department of Physiology, Medical College of Virginia, Virginia Commonwealth University, 1101 E. Marshall Street, Richmond, VA 23298, USA
e-mail: gtseng@vcu.edu

post-TMD regions (28–41% identical, 41–61% similar) (Teng et al., 2003). Whether the other KCNE subunits adopt an α-helical structure in their TMDs and how they modulate the function of their partner Kv channels are not clear. There appears to be a paradox. On the one hand, similar mutations introduced into equivalent positions in the post-TMD region of KCNE1, KCNE2 and KCNE3 have similar impact on the modulation of their respective partner Kv channels (Abbott & Goldstein, 2002), and swapping the residue at an equivalent TMD position between KCNE1 and KCNE3 can transfer the major effects on KCNQ1 activation kinetics (Melman, Krumerman & McDonald, 2002), suggesting that different KCNE subunits may use a similar mechanism to bind to and modulate their respective partner Kv channels. On the other hand, these KCNE subunits can have distinctly different effects even when they are associated with the same Kv channels (Bendahhou et al., 2005).

Our focus here is KCNE2 modulation of KCNQ1, which forms a background K conductance in acid-secreting parietal cells of the stomach (Roepke et al., 2006). We used cysteine (Cys)-scanning mutagenesis along the KCNE2 TMD (sequence and position numbers shown in Fig. 2a) to probe KCNQ1/KCNE2 interactions. Cysteine has a small hydrophobic side chain and is usually well tolerated in mutagenesis experiments, except where intimate interactions between protein residues or critical conformational changes occur. Therefore, perturbations of protein function by Cys substitution can be used to probe for "high-impact" positions that cannot tolerate side chain replacement by Cys (Liu et al., 2002). The major forces that stabilize the association between hydrophobic transmembrane α-helices are van der Waals interactions, which occur only when amino acid side chains are in close contact (Popot & Engelman, 2000). This is likely the case for the KCNQ1/KCNE2 complex, considering the highly hydrophobic nature of the KCNE2 TMD. Therefore, positions where Cys substitution perturbs KCNE2 modulation of KCNQ1 channel function are candidates for contact points between the two. Furthermore, the distribution pattern of high-impact positions may reveal the possible secondary structure adopted by this region (Liu et al., 2002). An α-helix with one face making intimate contacts with other protein domains (where side chain interactions influence protein function) and the other face exposed to membrane lipid or aqueous phase is likely to have high-impact positions at every third or fourth position, whereas a β-strand structure in the protein/lipid or protein/aqueous interface may have high-impact positions at every other position. There are other advantages of using Cys substitution to probe protein structure and function: Cys side chains can react with thiol-specific modifying reagents, and when two or more Cys side chains are in close proximity, they can coordinate a high-affinity binding site for Cd^{2+} or Zn^{2+} ions or form disulfide bonds. These often lead to perturbations of protein function, providing clues as to the locations of the Cys side chains and their relationship. However, scanning mutagenesis using alanine or tryptophan as the substituting residue can also lead to valuable information about the structure-function relationship of channel proteins.

Materials and Methods

Molecular Biology

Human KCNQ1 and KCNE2 clones were generous gifts from Drs. M. T. Keating (Harvard University, Cambridge, MA) and G. W. Abbott (Cornell University, Ithaca, NY). A c-myc tag is inserted between aa 20 and 21 in the extracellular domain of KCNE2, which does not affect its function as a Kv channel modulator (Zhang, Jiang & Tseng, 2001). We use the short KCNQ1 isoform (Sanguinetti et al., 1996), which is indistinguishable from the long KCNQ1 isoform (NCBI RefSeg: NP_000209) in terms of channel properties and KCNE modulation (Wu et al., 2006a) but is expressed more consistently in oocytes. KCNE2 cysteine substitution is created using an oligonucleotide-directed method (Alter Site II *In Vitro* Mutagenesis System; Promega, Madison, WI). A KCNQ1 mutation was created using the QuickChange mutagenesis kit (Stratagene, La Jolla, CA). All mutations were confirmed by direct DNA sequencing. Mutants were designated by wild-type (WT) residue, followed by position number; KCNQ1 position number was based on the long isoform, in keeping with previous publications (Melman et al., 2002; Tapper & George, 2001), and then by the substituting residue, using the one-letter aa code. For *in vitro* transcription, plasmids were linearized by suitable restriction enzymes and transcribed using a commercial kit (Mmessage Mmachine; Ambion, Austin, TX). The cRNA band sizes and intensities were quantified by densitometry of RNA gels stained with ethidium bromide (ChemiImager model 4400; Alpha Innotech, San Leandro, CA).

Oocyte Experiments

Stage V-VI oocytes were isolated from *Xenopus laevis* and incubated in an ND96-based medium (composition given below), supplemented with 4% horse serum and penicillin/streptomycin at 16°C. The scheme of cRNA injection is described in results. Whole-oocyte membrane currents were recorded using the '2-cushion' pipette voltage-clamp method (Schreibmayer, Lester & Dascal, 1994). Both current-passing and voltage-recording pipettes had tip resistance of 0.2-0.6 MΩ. During recordings, the oocyte was continuously superfused with a low-Cl ND96 solution to reduce interference from endogenous Cl channels. Ref-

erence half-cells were electrically connected to the bath solution via salt bridges made of 1% agarose in 3 M KCl to reduce liquid junction potential. Voltage clamp was done at room temperature (24–26°C) with OC-725B or OC-725C amplifier (Warner Instruments, Hamden, CT). Voltage-clamp protocol generation and data acquisition were controlled by pClamp5.5 via a 12-bit D/A and A/D converter (DMA; Axon Instruments, Burlingame, CA). Currents were low-pass filtered at 1 kHz (Frequency Devices, Haverhill, MA) and stored on disks for offline analysis.

The following solutions were used: (a) ND96 containing (in mM) NaCl 96, KCl 2, $CaCl_2$ 1.8, $MgCl_2$ 1, 4-(2-hydroxyethyl)-1-piperazineethanesulfonic acid (HEPES) 5, Na-pyruvate 2.5 (pH 7.5); (b) low-Cl ND96, in which Cl^- ions in ND96 were replaced by methanesulfonate; (c) 98 mM K, Rb or Cs ND96, in which Na^+ in low-Cl ND96 was replaced by 96 mM K^+, 98 mM Rb^+ or 98 mM Cs^+ (K^+ was omitted in the Rb^+ and Cs^+ solutions). Na-pyruvate was omitted in all three solutions.

Data Analysis

Voltage-clamp protocols and methods of data analysis are described in figure legends. The following software was used for data analysis: pClamp6 or 8, EXCEL (Microsoft, Redmond, WA); SigmaPlot, SigmaStat and PeakFit (SPSS, Chicago, IL). For multiple group comparison, data were analyzed by one-way analysis of variance and, if $p < 0.001$, followed by Dunn's test of multiple group comparison *vs.* a reference (WT KCNE2 data).

Oocyte Cell Surface Protein Biotinylation and Immunoblotting

Oocytes (30 per group) were rinsed with ND96 and incubated with 10 mg/ml sulfo-NHS-SS-biotin (Pierce) at 4°C two times for 20 min each. After thorough rinsing to remove unbound biotin, oocytes were homogenized in 200 mM NaCl and 20 mM Tris-HCl (pH 7.4) with protease inhibitor cocktail (Sigma-Aldrich, St. Louis, MO). After low-speed (1,500 rpm) centrifugation to remove debris, the oocyte lysate was solubilized by incubation in 1% Triton X-100 for 1 h on ice. After centrifugation to remove insoluble materials, the protein concentration in supernatant was measured. To retrieve biotinylated proteins, the supernatant was incubated with washed NeuAvidin beads (Pierce, at 50 µl beads per 200 µg protein) at 4°C overnight. Afterward, the beads were collected and biotinylated proteins were eluted by heating in sodium dodecyl sulfate (SDS) sample buffer containing 2-mercaptoethanol at 60°C for 30 min.

Protein samples of whole-cell lysate were heated to 60°C for 30 min in SDS sample buffer containing 2-mercaptoethanol and loaded onto 4–20% gradient SDS polyacrylamide gels along with the biotinylated fraction described above. After fractionation, proteins were blotted onto polyvinylidene difluoride (PVDF) membranes (Amersham, Arlington Heights, IL). Residual proteins in the gel were stained with Coomassie blue to check loading variations. The PVDF membranes were cut between 50- and 37-kDa size markers and blocked in phosphate-buffered saline (PBS) with 5% dry milk and 0.1% Tween-20 for 1 h at room temperature. The upper portion wa incubated with antibody against KCNQ1 (H-130; Santa Cruz Biotechnology, Santa Cruz, CA), and the lower portion was incubated with antibody against KCNE2 (Alomone, Jerusalem, Israel; catalog APC-054) at 4°C overnight. This was followed by rinsing in PBS with 0.1% Tween-20. The membranes were then incubated in diluted horseradish peroxidase-conjugated goat anti-rabbit immunoglobulin G (Amersham) for 1 h at room temperature. Immunoreactivity was visualized using an enhanced chemiluminescence detection kit (Amersham).

Results

KCNE2 Has Multiple Effects on KCNQ1

Coinjecting (KCN)E2 with (KCN)Q1 cRNA (10 ng each per oocyte, corresponding to a cRNA molar ratio of 3:1) revealed a marked current suppression effect (Fig. 1b, left panel). However, in these oocytes, the Q1 protein level was severely reduced (Fig. 1d, first and second panels, rightmost lanes; similar degree of Q1 protein reduction in both whole-cell and cell surface). On the other hand, delaying E2 cRNA injection by 2 days (Fig. 1a) still led to effective E2 protein expression (Fig. 1d, third panel) and Q1 modulation (Fig. 1b, right panel, and c), without significantly reducing Q1 protein level in the oocytes. It has been shown that E2 expressed alone (in Chinese hamster ovary cells) can effectively traffic to the cell surface (Isbrandt et al., 2002) (a situation apparently different from that of KCNE1 expression [Chandrasekhar, Bas & Kobertz, 2006]). Therefore, we suggest that E2 translated after delayed cRNA injection can traffic to the oocyte cell surface and associate with existing Q1 channels to modulate their function. As has been described previously (Wu et al., 2006a), E2 coexpression induces the following changes on Q1 gating kinetics: slowing activation, shifting the activation curve in the positive direction with reduced steepness, slowing deactivation and inducing a constitutive current component (Fig. 1b, right panel, and c).

In the following experiments, we compared in a quantitative manner the effects of WT E2 and Cys-substituted E2 mutants on Q1 channel function. We delayed E2 cRNA

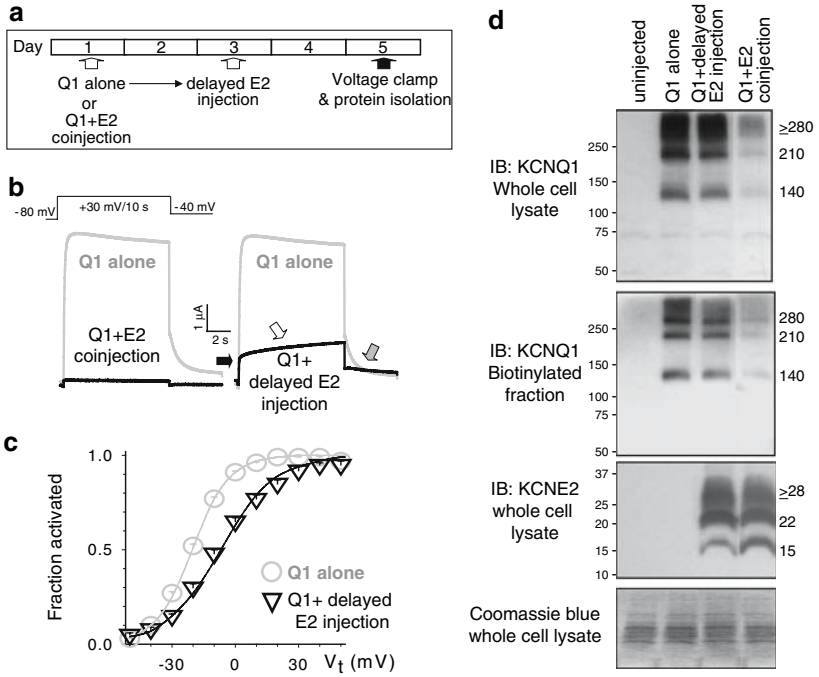

Fig. 1 Multiple effects of (KCN)E2 on (KCN)Q1. **a** Experimental schedule. Oocytes were isolated on day 1 and injected with cRNA for Q1 alone or Q1+E2 (Q1 10 ng/oocyte in both cases, E2 10 ng/oocyte in the latter case). Some of the Q1-injected oocytes were further injected with E2 cRNA (10 ng/oocyte) on day 3. On day 5, oocytes were subjected to voltage clamp (data in **b** and **c**) followed by protein isolation (data in **d**). **b** E2 reduces Q1 current amplitude and alters its gating kinetics. Shown are representative current traces elicited by the voltage-clamp protocol diagrammed on top from three oocytes: one injected with Q1 alone, one with Q1+E2 coinjection and one with Q1+delayed E2 injection. The same Q1 alone trace (*gray*) is superimposed with the Q1+E2 coinjection or Q1+delayed E2 injection trace (*black*) to illustrate the E2 effects. Test pulse currents were leak-subtracted and normalized by the mean current amplitude of Q1 alone oocytes. The average values are Q1 alone, 1.00 ± 0.12 (n = 10); Q1+E2 coinjection, 0.02 ± 0.006 (n = 11), Q1+delayed E2 injection, 0.39 ± 0.12 (n = 12). In the *right panel, black, white* and *gray arrows* point to the following features of the Q1+delayed E2 injection trace: initial current jump upon membrane depolarization (time-independent or constitutive component), slow activation and slow deactivation of the time-dependent component, respectively. **c** E2 shifts Q1 activation curve in the positive direction and reduces its steepness. The relationship between test pulse voltage (V_t) and peak tail current amplitude (I_{tail}) elicited by V_t was fit with a Boltzmann function: $I_{tail} = I_{max}/\{1 + \exp[z_g(V_{0.5}\text{-}V_t)F/RT]\}$, where I_{max} = extrapolated maximum I_{tail}, z_g = apparent gating charge, $V_{0.5}$ = half-maximum activation voltage, F = Faraday constant, R = gas constant and T = absolute temperature. For Q1+delayed E2 injection, only the time-dependent component was considered. Shown is fraction of channels activated (I_{tail}/I_{max}) plotted against V_t. The superimposed curves are calculated from the Boltzmann function, with the following average parameter values for $V_{0.5}$ and z_g: Q1 alone, 20.5 ± 0.4 mV and 2.88 ± 0.04 (n = 79); Q1+delayed E2 injection, 7.0 ± 1.2 and 2.02 ± 0.07 (n = 38). **d** E2 coinjection, but not delayed E2 injection, markedly reduced Q1 protein level in oocytes. Whole-cell lysate and biotinylated fraction were prepared from uninjected oocytes and oocytes injected with cRNA(s) (*listed on top*) and analyzed by immunoblotting (*IB*). *Bottom panel* is Coomassie blue stain of high-abundance proteins in the whole-cell lysate to confirm even loading of total proteins. Size marker positions are noted on the *left*. Q1- or E2-specific bands are marked on the *right*. Based on densitometric analysis and relative to the Q1 alone lane in the same gel, the Q1-band intensity in the Q1+delayed E2 injection lane is ~0.9, while the Q1-band intensity in the Q1+E2 coinjection lane is only 0.3 and 0.4 in whole-cell lysate and biotinylated fraction, respectively

injection to avoid potential interference by Q1 protein reduction in the quantification of the E2 current-suppressing effect. To further avoid excessive current suppression by some of the E2 mutants (*see below*), we adjusted the amount of E2 (WT and mutants) cRNA injected to 3.3 ng/oocyte. For proper data analysis and interpretation, we needed to distinguish currents through exogenously expressed Q1 channels modified by E2 (WT or mutants) from endogenous currents. We also needed to ensure that we were studying Q1 channels modified by the E2 subunits, instead of a heterogeneous channel pool containing unmodified (E2-free) Q1 channels. Experiments shown in Figures 2 and 3a address these issues.

Using HMR1556 to Identify Currents through Exogenous KCNQ1 Channels Modified by WT or Mutant KCNE2 Subunits

HMR1556 blocks Q1 with a 50% inhibition concentration (IC_{50}) of 0.4 μM (Lerche et al., 2000). When tested on Q1 coexpressed with E2 WT or mutants, 10 μM HMR produced the maximal degree of current suppression

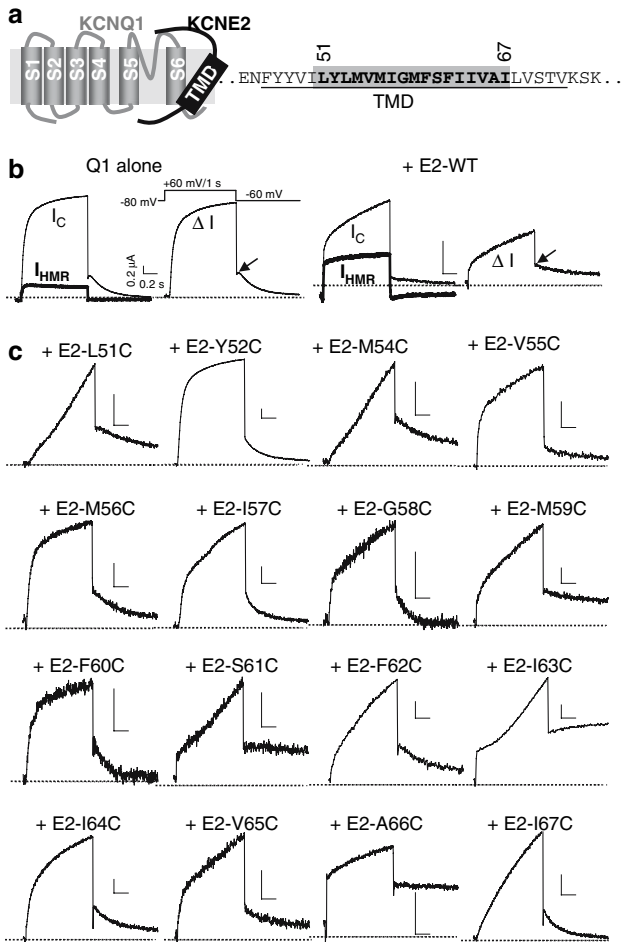

Fig. 2 Using HMR1556 (HMR) to identify currents through exogenous KCNQ1 channels modulated by coexpressed KCNE2 subunits. In experiments shown here and in Figures 3–5, E2 cRNA (3.3 ng/oocyte) was injected 2 days after Q1 cRNA (10 ng/oocyte) injection. **a** *Left*: Diagram of transmembrane topology of KCNQ1 and KCNE2 subunits. *Right*: Amino acid sequence of KCNE2 TMD (*underlined*) and flanking regions. Positions examined in this study are highlighted in *gray*, with position numbers of the two ends denoted. **b** Effects of HMR (10 μM) on Q1 alone or Q1 coexpressed with WT E2 (+E2-WT). For each panel, the left part shows currents recorded under control conditions (I_C, *thin traces*) and at the steady state of HMR suppression (I_{HMR}, *thick traces*). The right part shows HMR-sensitive currents ($\Delta I = I_C - I_{HMR}$). Voltage-clamp protocol is diagrammed on *top*. *Arrows* point to the peak of tail current in ΔI traces, manifesting a rising phase (hook) in Q1 alone but not in +E2-WT. **c** HMR-sensitive currents recorded from oocytes coexpressing Q1 with Cys-substituted E2 mutants (marked for each panel). The voltage-clamp protocol, HMR application and data analysis are the same as those described for **b**. For all panels, the calibration bars represent 0.2 μA and 0.2 s and the *dotted horizontal lines* denote the zero current level

(increasing drug concentration to 50 μM did not lead to further effects, *data not shown*). HMR at 10 μM did not affect currents in uninjected oocytes (Wu et al., 2006a), although it did suppress I_{Ks} currents in oocytes injected with KCNE1 cRNA alone (that form I_{Ks} with oocyte endogenous xKCNQ1) (Sanguinetti et al., 1996) (*data not shown*). This suggests that the endogenous xKCNQ1 channel activity alone is too low for detection and other oocyte endogenous channels are insensitive to HMR. Therefore, we used currents suppressed by 10 μM HMR (HMR-sensitive current or ΔI, Fig. 2b,c) as an indication of currents through exogenous Q1 channels.

Figure 2b shows that the HMR-sensitive current recorded from an oocyte coexpressing Q1 and E2-WT bears all the characteristics of E2-modified Q1 channels (Wu et al., 2006a): the holding current level is above 0 (V_h –80 m*V*, positive to expected E_K of –95 m*V*), and there is a prominent instantaneous current jump upon membrane depolarization, both signifying a constitutively active channel component. The remaining time-dependent current shows slowed activation and deactivation (compare ΔI of Q1 alone *vs.* +E2-WT). The rising phase of the tail current (hook), consistently manifested by Q1 expressed alone, is missing in Q1+E2-WT (arrows of ΔI traces in Fig. 2b), indicating that E2 removes Q1 inactivation.

Figure 2c depicts HMR-sensitive currents recorded from oocytes coexpressing Q1 with E2 mutants. Except for E2-Y52C, all the other current traces are substantially different from Q1 expressed alone. Although the waveform of Q1+E2-Y52C appears similar to that of Q1 expressed alone, the midpoint of its activation curve is actually shifted rightward by >20 m*V* (*see* Fig. 3a). We could not detect HMR-sensitive currents from four batches of oocytes coexpressing Q1 with E2-L53C. However, coexpressing E2-L53C with Kv4.2 (another E2 partner Kv channel [Zhang et al., 2001]) induced distinct effects on the Kv4.2 gating kinetics similar to those induced by WT-E2 (*data not shown*). These observations indicate that E2-L53C is a functional E2 subunit that appears to be a uniquely potent Q1 current suppressor.

Note that current traces in the presence of 10 μM HMR are not totally time-independent (Fig. 2b, traces marked by I_{HMR}). This may reflect oocyte native currents as well as time-dependent HMR block and unblock during voltage-clamp pulses. We did not investigate these possibilities thoroughly. However, it is important to point out that using the maximally effective HMR concentration to obtain HMR-sensitive currents in our experiments represents the best strategy currently available to monitor the effects of WT or mutant KCNE2 on KCNQ1.

Two observations in Figure 2 suggest that there was little interference by E2-free Q1 channels in these experiments. First, like E2-WT, all the E2 mutants (excluding E2-L53C) effectively suppressed Q1 inactivation. If there were unmodified Q1 channels present in these oocytes, they would manifest a hook phase in the tail currents. This was not the case. Second, for those E2 mutants (e.g., L51C, M54C, and I67C) that markedly slowed Q1 activation and suppressed Q1 current ampli-

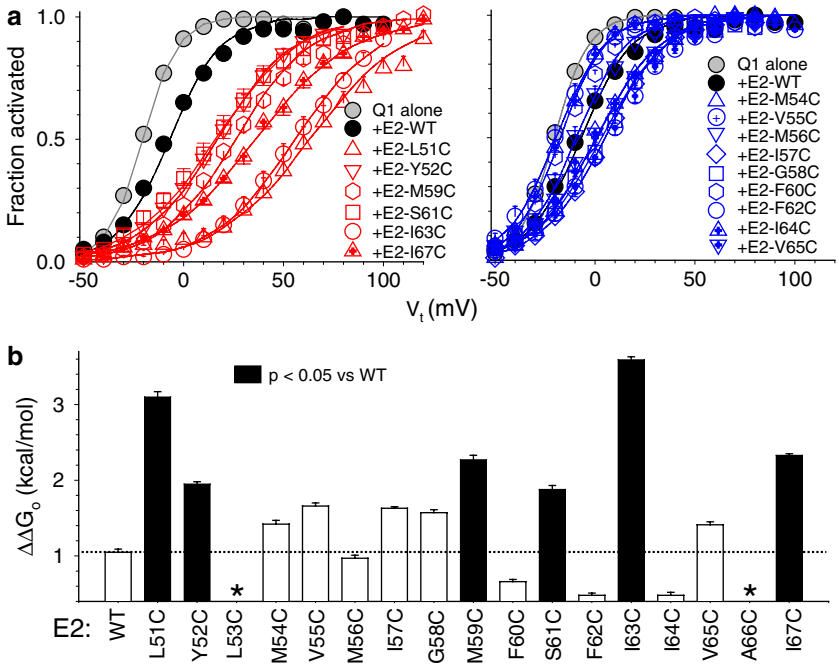

Fig. 3 Pattern of perturbation by Cys substitution of KCNE2 modulation of KCNQ1's voltage dependence of activation. The voltage-clamp protocol and data analysis are the same as those described for Figure 1**c**. In E2 coexpressed oocytes, only the time-dependent current component was used for analysis. **a** Superimposed activation curves for Q1 alone and Q1+E2-WT or Q1+E2 mutants. Data from E2 mutants whose effects are significantly different from those of E2-WT are shown in the *left panel* (*red symbols/curves*), and mutants whose effects are not significantly different from those of E2-WT are shown in the *right panel* (*blue symbols/curves*). **b** Effects of E2-WT and mutants on the energetics of Q1 activation. Assuming a two-state (closed and open) gating scheme, the free energy of Q1 channel activation at 0 m*V*, ΔG_o, is calculated as $z_g V_{0.5} F$ (in kcal/mol), where z_g and $V_{0.5}$ are parameters from the Boltzmann fit (Fig. 1 legend) and F is the Faraday constant. E2-WT- or mutant-induced change in ΔG_o was calculated as $\Delta\Delta G_o = \Delta G_o^{Q1+E2} - \Delta G_o^{Q1}$, where ΔG_o^{Q1+E2} and ΔG_o^{Q1} are ΔG_o values for Q1 coexpressed with E2 or Q1 alone. The $\Delta\Delta G_o$ values are plotted against E2 types along the abscissa (n = 4–38 per group). Filled histogram bars, $p < 0.05$ E2-mutant *vs.* E2-WT. *No data for E2-L53C (no detectable currents) or E2-A66C (rarely time-dependent current component)

tude (*see* Fig. 4a), if there were unmodified Q1 channels with a relatively fast activation rate and unsuppressed current amplitude, we expected to see a fast-activating current component reflecting E2-free Q1 channels. No such component was discernable.

Some KCNE2 Mutants Cause a Marked Rightward Shift in the KCNQ1 Activation Curve

Figure 3a shows that six of the E2 mutants (L51C, Y52C, M59C, S61C, I63C and I67C) markedly shifted the voltage dependence of Q1 activation in the positive direction, and except M59C and I63C, they also greatly suppressed the Q1 current amplitude (*see* Fig. 4a). If there were unmodified Q1 channels present in these oocytes, with a relatively negative voltage range of activation and unsuppressed current amplitude, we expected to see a negative component of channel activation reflecting E2-free Q1 channels. No such component was discernable. Taken together, we conclude that under our experimental conditions we were observing Q1 channels modified by E2-WT or mutants with little interference from E2-free Q1.

Pattern of Cys Substitution-Induced Perturbation of KCNE2 Effect on KCNQ1 Current Amplitude

Figure 4a compares current amplitudes in oocytes expressing Q1 alone and Q1 coexpressed with E2-WT or mutants. The amplitudes are measured from peak tail currents elicited by 1-s test pulses to the plateau voltage of each channel's activation curve (to avoid interference due to different degrees of shift in the voltage range of activation) and recorded at –60 m*V* (to maintain the same driving force for currents through the channels). The degree of the E2 current-suppressing effect was reduced by Y52C, M56C, M59C and I63C. In particular, E2-I63C increased the Q1 current amplitude to above that of Q1 expressed alone.

Pattern of Cys Substitution-Induced Perturbation of KCNE2 Effect on KCNQ1 Pore Properties

We examined the effects of E2 WT and mutants on Q1 pore properties by measuring the profile of pore conductance to K^+, Rb^+ and Cs^+ ions and the Rb^+ to K^+ perme-

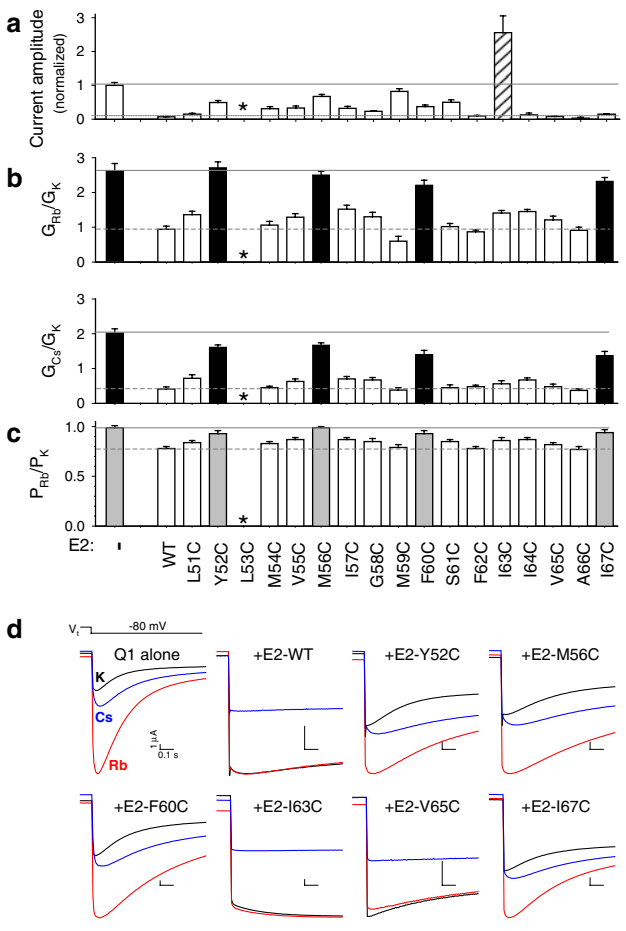

Fig. 4 Pattern of perturbation by Cys substitution of KCNE2 modulation of KCNQ1's pore properties. **a** Effects of E2-WT and mutants on Q1 current amplitude. Channels are activated by 1-s depolarization pulses to the plateau level of their activation curves (ranging from +40 to +120 m*V*, see Fig. 3**a**). Peak amplitudes of tail currents recorded upon repolarization to -60 m*V* were normalized by the mean value from Q1 alone oocytes. *Hatched bar*: E2-I63C coexpression increased Q1 current amplitude to above that of Q1 expressed alone. **b** Ratios of Rb^+ or Cs^+ chord conductance to K^+ chord conductance (G_{Rb}/G_K or G_{Cs}/G_K, see below for calculation). **c** Permeability ratio of Rb^+ to K^+ (P_{Rb}/P_K) (see below for calculation). In **b** and **c**, *black* and *gray histogram bars* denote Cys substitutions that remove the E2-WT effect on the Q1 pore ion conductance or permeability ratio ($p < 0.05$, E2-mutant *vs.* E2-WT). To facilitate data comparison, *solid* and *dashed gray lines* mark the data of Q1 alone and Q1+E2-WT, respectively. Data are plotted against Q1 alone (*leftmost histogram bar*, denoted by "- E2") and the type of E2 subunit (WT or Cys mutants, labeled along abscissa, n = 4-13 per group). *No detectable HMR-sensitive currents in Q1+E2-L53C oocytes. **d** Representative inward tail current traces recorded from oocytes expressing Q1 alone or with E2-WT or mutants (labeled for each panel). The voltage-clamp protocol is diagrammed on top: channels were activated by 1-s depolarization pulses to V_t that reaches the plateau of their activation curves (Fig. 3**a**), and tail currents were recorded upon repolarization to -80 m*V*. The tail currents were carried by K^+, Rb^+ or Cs^+ ions (recorded in 98 mM K^+, Rb^+ or Cs^+ bath solution) and color-coded *black, red* and *blue*, respectively. For all panels, calibration bars represent 1 μA and 0.1 s. The chord conductance is calculated by dividing peak amplitude of inward tail current recorded in 98 mM K^+, Rb^+ or Cs^+ by the driving force (difference between -80 m*V* and E_{rev}, where E_{rev} is reversal potential measured in respective ion solution). P_{Rb}/P_K is calculated from the shift in E_{rev} when bath solution was switched from 98 mM K^+ to 98 mM Rb^+ based on the constant-field equation: $P_{Rb}/P_K = \exp[(RT/F)(E_{Rb} - E_K)]$

ability ratio (P_{Rb}/P_K). Recordings were made in bath solutions containing 98 mM K^+, Rb^+ or Cs^+, without other monovalent cations and with low millimolar divalent cations. Amplitudes of inward tail currents carried by extracellular K^+, Rb^+ or Cs^+ ions (Fig. 4d) were divided by the driving force to obtain the chord conductance. For each cell, the Rb^+ or Cs^+ chord conductance was normalized by K^+ chord conductance and the conductance ratios (G_{Rb}/G_K and G_{Cs}/G_K) were averaged over cells (Fig. 4b). Unlike most K channels that have a conductance profile of $G_K \geq G_{Rb} > G_{Cs}$ (LeMasurier, Heginbotham & Miller, 2001; Morais Cabral, Zhou & MacKinnon, 2001), Q1 expressed alone exhibited a conductance profile of $G_{Rb} > G_{Cs} > G_K$: the G_{Rb}/G_K and G_{Cs}/G_K values were 2.63 ± 0.20 and 2.02 ± 0.12, respectively (Fig. 4b, leftmost histogram bars). The P_{Rb}/P_K value was 0.99 ± 0.02 for Q1 expressed alone (Fig. 4c). For Q1 coexpressed with E2-WT, the G_{Rb}/G_K and G_{Cs}/G_K values were 0.94 ± 0.09 and 0.41 ± 0.06 and the P_{Rb}/P_K value was 0.78 ± 0.02 (Fig. 4b,c; $p < 0.05$ Q1+E2-WT *vs.* Q1 alone for all three parameters). Thus, E2 modified the Q1 pore conductance profile (to make it similar to that of most other K channels) and reduced the P_{Rb}/P_K value of the Q1 channel pore.

We applied the same type of analysis to E2 mutants. Representative current traces from Q1 coexpressed with selected E2 mutants are shown in Figure 4d, and data are summarized in Figure 4b and c. Cys substitution at positions 52, 56, 60 and 67 clearly removed the E2 effect on Q1 pore properties: conductance profile was reverted to $G_{Rb} > G_{Cs} > G_K$, and the P_{Rb}/P_K values rose to that of Q1 expressed alone. At least part of this pattern of high-impact positions (positions 52-60) suggests an α-helical periodicity.

Pattern of Cys Substitution-Induced Perturbation of KCNE2 Effect on the Voltage Dependence of KCNQ1 Activation

The data shown in Figure 3a are fit with a simple Boltzmann function to obtain two parameter values: half-maximum activation voltage ($V_{0.5}$) and equivalent gating charge of activation (z_g). Because E2 WT and several mutants affect not only $V_{0.5}$ but also z_g, we used a composite parameter, ΔG_o (equivalent free energy of channel activation at 0 m*V*) to evaluate the E2 effects on Q1 gating. This parameter is based on the assumption of a two-state (closed and open) gating model. Although this is an oversimplification of how channels gate, this parameter takes into ac-

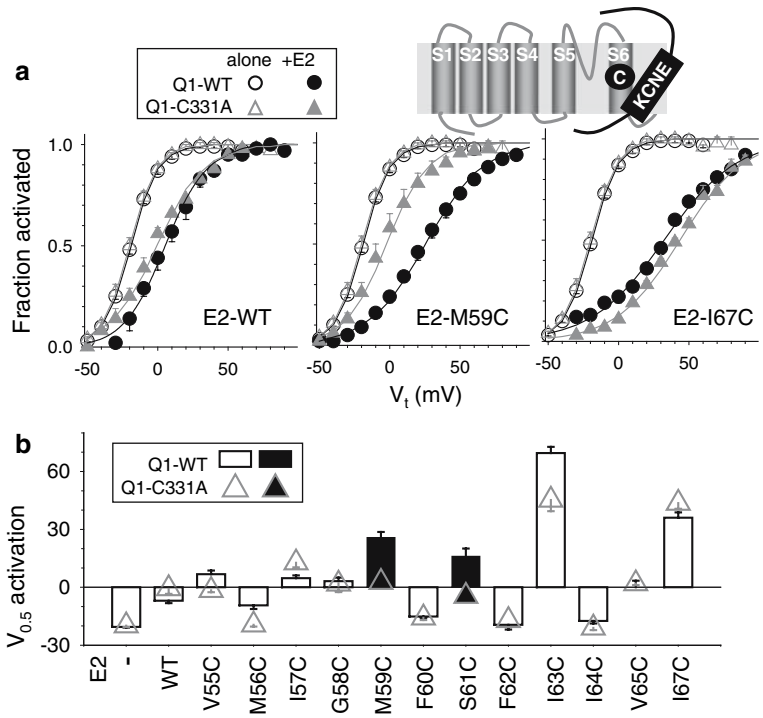

Fig. 5 Impact of KCNQ1 C331A mutation on KCNE2-induced shift in $V_{0.5}$ of activation. *Top right*: Two-dimensional diagram of Q1 and E2 subunits, with C(331) on Q1's S6 marked. *Top left*: Legend for symbols used in **a**. **a** Activation curves of Q1-WT (*circles*) and Q1-C331A (*triangles*) expressed alone (*open symbols*) or coexpressed with one of three E2 subunits (*filled symbols*): WT (*left*), M59C (*middle*) or I67C (*right*). **b** $V_{0.5}$ values of Q1-WT (*histogram bars*) or Q1-C331A (*triangles*) expressed alone (-E2, leftmost data points) or with E2 WT or mutants (listed along the abscissa). *Open histogram bars* and *triangles* indicate that there is no significant difference in the $V_{0.5}$ values between Q1-WT and Q1-C331A when they are expressed alone (-E2) or coexpressed with E2-WT or most of the E2 mutants. *Filled histogram bars* and *triangles* indicate that the $V_{0.5}$ values are significantly different between Q1-WT and Q1-C331A when they are coexpressed with E2-M59C or E2-S61C

count of both $V_{0.5}$ and z_g values and has been successfully used to identify the pattern of changes in channel gating caused by mutations (Zhang et al., 2005). Figure 3b summarizes the changes in ΔG_o ($\Delta\Delta G_o$) of Q1 activation gating caused by E2-WT and mutants. Among the mutants, L51C, Y52C, M59C, S61C, I63C and I67C increase the $\Delta\Delta G_o$ value much more than that induced by E2-WT. This pattern of high-impact positions is different from those shown in Figure 4a–c. However, such differences are expected if the contact points between E2 and Q1 involved in the modulation of Q1 gating kinetics differ from those involved in the modulation of Q1 pore properties (*see below*).

Impact of a KCNQ1 Mutation, C331A, on the Degree of $V_{0.5}$ Shift Caused by KCNE2 WT and Mutants

It has been suggested that in a (KCN)Q1/(KCN)E1 channel complex, a native cysteine on the Q1 S6 (C331) is close to the side chains at positions 54 and 55 on the E1 TMD (Tapper & George, 2001). To explore whether this is also the case for E2 association with Q1, we mutated C331 to alanine (Q1-C331A) and studied how this mutation impacts on the ability of E2-WT and mutants to shift the $V_{0.5}$ of Q1 activation. When expressed alone, the C331A mutation had no discernable effects on Q1 channel function (Fig. 5a, open symbols). When Q1-C331A was coexpressed with E2-WT, the degree of $V_{0.5}$ shift was essentially the same as that seen with Q1-WT (Fig. 5a, left panel). However, when Q1-C331A was coexpressed with E2-M59C, the degree of $V_{0.5}$ shift was markedly reduced relative to that seen with Q1-WT (Fig. 5a, middle panel, gray solid triangles *vs.* black solid circles). This difference between E2-WT and E2-M59C cannot be explained by the more pronounced positive shift in $V_{0.5}$ caused by the M59C mutation. For example, E2-I67C induced an even more pronounced positive shift in $V_{0.5}$ than E2-M59C. However, it was equally effective in shifting the $V_{0.5}$ of Q1-C331A as with Q1-WT (Fig. 5a, right panel). Figure 5b summarizes the data on $V_{0.5}$ of activation when Q1-WT or Q1-C331A was expressed alone, with E2-WT or with E2 mutants. For E2-WT and most of the mutants, the degrees of $V_{0.5}$ shift were the same or very similar between Q1-WT and Q1-C331A (i.e., overlapping values denoted by open histogram bars and open triangles). There were two exceptions: the amount of $V_{0.5}$ shift caused by E2-M59C and E2-S61C in Q1-C331A was significantly less than that caused by the two mutants in Q1-WT. These observations

suggest that residues at E2 positions 59 and 61 are functionally coupled to Q1 position 331.

Discussion

This is the first systematic characterization of how Cys substitutions along a KCNE subunit's TMD can perturb the modulation of its partner Kv channel. Similar Cys substitutions along KCNE1's TMD have been described in landmark papers published by Goldstein's group (Wang et al., 1996; Tai & Goldstein, 1998). However, those Cys mutants were mainly used to probe for Methane thiosulfonate (MTS) or Cd^{2+} modification of KCNE1/KCNQ1 interactions, instead of probing for the impact of Cys substitution per se on KCNE1/KCNQ1 interaction. We report the novel finding of high-impact positions on the KCNE2 TMD where Cys substitution markedly affects KCNE2 modulation of KCNQ1 channel function. However, the distribution pattern of these high-impact positions depends on whether KCNQ1 current amplitude, ion selectivity or gating kinetics is considered. These observations suggest that modulation of these different aspects of KCNQ1 channel function involves different sets of contact points between KCNQ1 and KCNE2.

The transmembrane regions of membrane proteins adopt one of two secondary structures to shield their hydrophilic peptide backbones from the hydrophobic lipid environment: α-helix or β-sheet. Previously an NMR spectroscopic study showed that a peptide corresponding to the TMD of KCNE1 adopts an α-helical structure when placed in a solvent comprising 86% v/v 1,1,1,3,3,3-hexafluoro-isopropanol and 14% v/v water (Aggeli et al., 1998). The amino acid sequence of the KCNE2 TMD is highly homologous to that of KCNE1 (Fig. 6a). Indeed, a Fourier transform infrared spectroscopic study also suggested that a peptide corresponding to the KCNE2 TMD contains a stable α-helical structure(s) when placed in detergent micelles (G. W. Abbott, *personal communication*). Therefore, in the following text, we discuss our observations in the context of a KCNE2 transmembrane helix.

Pattern of Perturbation by Cys Substitution of KCNQ1/KCNE2 Pore Properties

Cys substitutions at KCNE2 positions 52, 56, 60 and 67 change the conductance profile of the KCNQ1/KCNE2 channel pore and the P_{Rb}/P_K value so that they resemble those of KCNQ1 expressed alone. Cys substitution at position 63 uniquely increases the current amplitude of KCNQ1/KCNE2 channels to above that of KCNQ1 expressed alone. Therefore, the distribution pattern of high-impact positions in terms of perturbation of KCNE2

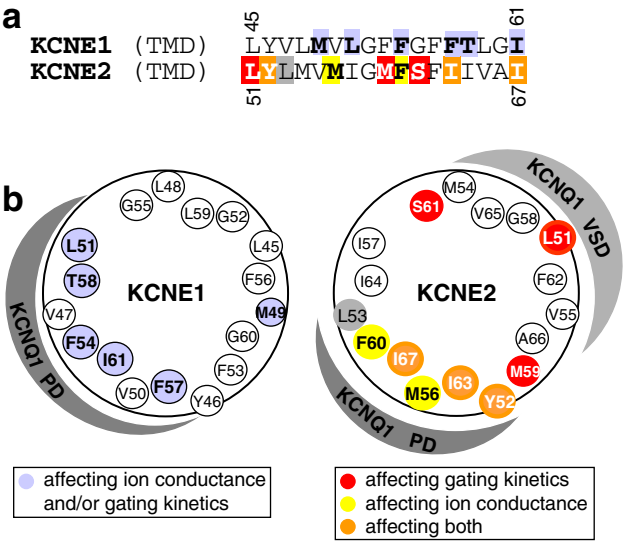

Fig. 6 Comparison of putative interaction surface of KCNE1 and KCNE2 when associated with KCNQ1. **a** Amino acid sequence alignment of KCNE1 and KCNE2 TMD. Residues are highlighted in the same colors as in **b**. **b** KCNE1 and KCNE2 TMDs are shown in a helical wheel format, viewed from the N-terminal (extracellular) end. KCNE1 residues where mutations affect ion conductance/selectivity and/or gating kinetics of associated KCNQ1 channels (Aggeli et al., 1998) are highlighted in *light blue*, and this KCNE1 surface is proposed to interact with the KCNQ1 pore domain (*PD*). The putative surfaces of KCNE2 interacting with KCNQ1's pore domain and voltage-sensing domain (*VSD*) are assigned based on whether Cys substitution affects ion conductance only (*yellow*), voltage dependence of activation only (*red*) or both (*orange*). L53 is highlighted in *gray* because it totally suppresses Q1 current

modulation of KCNQ1 pore properties (52, 56, 60, 63 and 67) exhibits an α-helical periodicity. This is consistent with a scenario in which the KCNE2 TMD adopts an α-helical structure with one face making intimate contacts with the KCNQ1 pore domain, and Cys substitutions of KCNE2 residues on this interaction surface perturb the KCNQ1 pore properties.

Pattern of Perturbation by Cys Substitution of KCNQ1/KCNE2 Gating Energetics

KCNE2 induces two apparently opposing effects on KCNQ1 gating kinetics. On the one hand, KCNE2 makes the KCNQ1 activation gate more reluctant to open, shown by the slowing of activation and the shift of the activation curve to a more positive voltage range. On the other hand, KCNE2 makes the KCNQ1 activation gate more reluctant to close, shown by the slowing of deactivation and induction of a constitutively active current component. These apparently opposing effects can be reconciled by proposing that KCNE2 association with the KCNQ1 channel reduces the efficiency of coupling between the S4 in KCNQ1's voltage-sensing domain and the activation gate in

KCNQ1's pore domain (Lu, Klem & Ramu, 2002; Long, Campbell & MacKinnon, 2005). It has been suggested that in a KCNQ1/KCNE1 channel complex, KCNE1 functionally interacts with two regions of KCNQ1's voltage-sensing domain: the outer end of S1 close to the extracellular cell surface (Chen et al., 2003; Hong et al., 2005) and the S4-S5 linker close to the intracellular cell surface (Franqueza et al., 1999). In our experiments, positions where Cys substitutions perturb KCNQ1 gating kinetics cluster to the extracellular end and cytoplasmic half of KCNE2's TMD. Future experiments will determine whether the contact points between the KCNE2 TMD and the KCNQ1 voltage-sensing domain are similar to those proposed for the KCNQ1/KCNE1 channel complex.

Comparing KCNE2 and KCNE1 in How They Interact with the KCNQ1 Channel

KCNE2 is similar to KCNE1 in its ability to slow KCNQ1 activation, shift the activation curve in the positive direction and suppress KCNQ1 inactivation. However, KCNE2 is distinctly different from KCNE1 in its suppression of current amplitude through the KCNQ1 channels and in hindering KCNQ1 deactivation. How similar is the conformation of these two KCNE subunits in a KCNQ1/KCNE channel complex? Figure 6a shows an amino acid sequence alignment of KCNE1 and KCNE2 in the TMD region. The two are 35% identical and 53% similar. Based on this high degree of homology, we can compare the distribution pattern of high-impact positions identified for KCNE1 (Takumi et al., 1991; Goldstein & Miller, 1991; Wilson et al., 1994) and for KCNE2 (present study) on the TM helices (Fig. 6b). The comparison suggests a similar orientation of KCNE1 and KCNE2 TM helices with respect to KCNQ1. However, mutations at positions 51 and 58 of KCNE1 can affect KCNQ1 current amplitude (Takumi et al., 1991), while mutations at the equivalent KCNE2 positions (57 and 64) are relatively inert (present study). It is as if the KCNE1 TMD rotates ~20^{o} counterclockwise relative to the KCNE2 TMD in interacting with KCNQ1. Figure 6a indicates that M59/S61 of KCNE2 (which are functionally coupled to C331 of KCNQ1) are at about the same position as F54/G55 of KCNE1 (which are close to C331 of KCNQ1) (Tapper & George, 2001). (It is not clear how positions at different faces of a KCNE TM helix, F54/G55 of KCNE1 and M59/S61 of KCNE2, can interact with the same residue, C331, on KCNQ1; one possible explanation is that there is a rotation of the KCNE TM helices relative to KCNQ1 during gating.) Furthermore, KCNE2 position 63 (where Cys substitution markedly impacts KCNQ1 activation kinetics) is equivalent to KCNE1 position 57, which is the first one of the activation triplet involved in modulating KCNQ1 activation kinetics (Melman et al., 2001). These similarities suggest that KCNE1 and KCNE2 TM helices are at a similar position and have a similar orientation with respect to KCNQ1 in a KCNQ1/KCNE channel complex. The observation that a single point mutation on KCNE2, I63C, can change the KCNQ1/KCNE2 channel phenotype to KCNQ1/KCNE1-like (increased current amplitude, slow activation and positive shift in the activation curve) suggests that the major determinant for the different outcomes of KCNE1 *vs.* KCNE2 modulation of KCNQ1 channel function is probably the physicochemical properties and geometries of side chains at contact points between KCNQ1 and the KCNE subunits.

Acknowledgement This work was supported by HL 67840 and HL 46451 from National Heart, Lung and Blood Institute of the National Institutes of Health (to G. N. T.) and a grant-in-aid award from American Heart Association/Mid-Atlantic Affiliate (to M. Z.).

References

Abbott GW, Goldstein SAN (1998) A superfamily of small potassium channel subunits: form and function of the MinK-related peptides (MiRPs). Q Rev Biophys 31:357–398

Abbott GW, Goldstein SAN (2002) Disease-associated mutations in *KCNE* potassium channel subunits (MiRPs) reveal promiscuous disruption of multiple currents and conservation of mechanism. FASEB J 16:390–400

Aggeli A, Bannister ML, Bell M, Boden N, Findlay JBC, Hunter M, Knowles PF, Yang J-C (1998) Conformation and ion-channeling activity of a 27-residue peptide modeled on the single-transmembrane segment of the IsK (minK) protein. Biochemistry 37:8121–8131

Bendahhou S, Marionneau C, Haurogne K, Larroque M-M, Derand R, Szuts V, Escande D, Demolombe S, Barhanin J (2005) In vitro molecular interactions and distribution of KCNE family with KCNQ1 in the human heart. Cardiovasc Res 67:529–538

Chandrasekhar KD, Bas T, Kobertz WR (2006) KCNE1 subunits require co-assembly with K^+ channels for efficient trafficking and cell surface expression. J Biol Chem 281:40015–40023

Chen Y-H, Xu S-J, Bendahhou S, Wang X-L, Wang Y, Xu W-Y, Jin H-W, Sun H, Su X-Y, Zhuang Q-N, Yang Y-Q, Li Y-B, Liu Y, Xu H-J, Li X-F, Ma N, Mou C-P, Chen Z, Barhanin J, Huang W (2003) KCNQ1 gain-of-function mutation in familial atrial fibrillation. Science 299:251–254

Franqueza L, Lin M, Shen J, Keating MT, Sanguinetti MC (1999) Long QT syndrome-associated mutations in the S4-S5 linker of KvLQT1 potassium channels modify gating and interaction with minK subunits. J Biol Chem 274:21063–21070

Goldstein SAN, Miller C (1991) Site-specific mutations in a minimal voltage-dependent K^+ channel alter ion selectivity and open-channel block. Neuron 7:403–408

Hong K, Piper DR, Diaz-Valdecantos A, Brugada J, Oliva A, Burashnikov E, Santos-de-Soto J, Grueso-Montero J, Diaz-Enfante E, Brugada P, Saches F, Sanguinetti MC, Brugada R (2005) De novo KCNQ1 mutation responsible for atrial fibrillation and short QT syndrome in utero. Cardiovasc Res 68:433–440

Isbrandt D, Friederich P, Solth A, Haverkamp W, Ebneth A, Borggrefe M, Funke H, Sauter K, Breithardt G, Pongs O,

Schulze-Bahr E (2002) Identification and functional characterization of a novel KCNE2 (MiRP1) mutation that alters HERG channel kinetics. J Mol Med 80:524–532

LeMasurier M, Heginbotham L, Miller C (2001) KcsA: it's a potassium channel. J Gen Physiol 118:303–313

Lerche C, Seebohm G, Wagner C, Scherer CR, Dehmelt L, Abitbol I, Gerlach U, Brendel J, Attali B, Busch AE (2000) Molecular impact of minK on the enantiospecific block of I_{Ks} by chromanols. Br J Pharmacol 131:1503–1506

Liu J, Zhang M, Jiang M, Tseng G-N (2002) Structural and functional role of the extracellular S5-P linker in the HERG potassium channel. J Gen Physiol 120:723–737

Long SB, Campbell EB, MacKinnon R (2005) Voltage sensor of Kv1.2: structural basis of electromechanical coupling. Science 309:903–908

Lu Z, Klem AM, Ramu Y (2002) Coupling between voltage sensors and activation gate in voltage-gated K^+ channels. J Gen Physiol 120:663–676

Melman YF, Demenech A, de la Luna S, McDonald TV (2001) Structural determinants of KvLQT1 control by the KCNE1 family of proteins. J Biol Chem 276:6439–6444

Melman YF, Krumerman A, McDonald TV (2002) A single transmembrane site in the KCNE-encoded proteins controls the specificity of KvLQT1 channel gating. J Biol Chem 277:25187–25194

Morais Cabral JH, Zhou Y, MacKinnon R (2001) Energetic optimization of ion conduction rate by the K^+ selectivity filter. Nature 414:37–42

Popot J-L, Engelman DM (2000) Helical membrane protein folding, stability, and evolution. Annu Rev Biochem 69:881–922

Roepke TK, Anantharam A, Kirchhof P, Busque SM, Young JB, Geibel JP, Lerner DJ, Abbott GW (2006) The KCNE2 potassium channel ancillary subunit is essential for gastric acid secretion. J Biol Chem 281:23740–23747

Sanguinetti MC, Curran ME, Zou A, Shen J, Spector PS, Atkinson DL, Keating MT (1996) Coassembly of KvLQT1 and minK (IsK) proteins to form cardiac I_{Ks} potassium channel. Nature 384:80–83

Schreibmayer W, Lester HA, Dascal N (1994) Voltage clamping of *Xenopus laevis* oocytes utilizing agarose-cushion electrodes. Pfluegers Archiv 426:453–458

Sesti F, Goldstein SAN (1998) Single-channel characteristics of wild-type I_{Ks} channels and channels formed with two minK mutants that cause long QT syndrome. J Gen Physiol 112:651–663

Tai KK, Goldstein SAN (1998) The conduction pore of a cardiac potassium channel. Nature 391:605–608

Takumi T, Moriyoshi K, Aramori I, Ishii T, Oiki S, Okada Y, Ohkubo H, Nakanishi S (1991) Alteration of channel activities and gating by mutations of slow I_{SK} potassium channel. J Biol Chem 266:22192–22198

Tapper AR, George AL Jr (2000) MinK subdomains that mediate modulation of and association with KvLQT1. J Gen Physiol 116:379–390

Tapper AR, George AL Jr (2001) Location and orientation of minK within the I_{Ks} potassium channel complex. J Biol Chem 276:38249–38254

Teng S, Ma L, Zhen Y, Lin C-X, Bahring R, Vardanyan V, Pongs O, Hui R (2003) Novel gene *hKCNE4* slows the activation of the KCNQ1 channel. Biochem Biophys Res Commun 303:808–813

Wang K-W, Tai KK, Goldstein SAN (1996) MinK residues line a potassium channel pore. Neuron 16:571–577

Wilson GG, Sivaprasadarao A, Findlay JBC, Wray D (1994) Changes in activation gating of I_{sK} potassium currents brought about by mutations in the transmembrane sequence. FEBS Lett 353:251–254

Wu D-M, Jiang M, Zhang M, Liu X-S, Korolkova YV, Tseng G-N (2006a) KCNE2 is colocalized with KCNQ1 and KCNE1 in cardiac myocytes and may function as a negative modulator of I_{Ks} current amplitude in the heart. Heart Rhythm 3:1469–1480

Wu D-M, Lai L-P, Zhang M, Wang H-L, Jiang M, Liu X-S, Tseng G-N (2006b) Characterization of an LQT5-related mutation in KCNE1, Y81C: implications for a role of KCNE1 cytoplasmic domain in I_{Ks} channel function. Heart Rhythm 3:1031–1040

Zhang M, Jiang M, Tseng G-N (2001) MinK-related peptide 1 associates with Kv4.2 and modulates its gating function. A potential role as ß subunit of cardiac transient outward channel. Circ Res 88:1012–1019

Zhang M, Liu J, Jiang M, Wu DM, Sonawane K, Guy HR, Tseng G-N (2005) Interactions between charged residues in the transmembrane segments of voltage-sensing domain of the hERG channel. J Membr Biol 207:169–181